# Loss of OMA1 delays neurodegeneration by preventing stress-induced OPA1 processing in mitochondria

Anne Korwitz,[1] Carsten Merkwirth,[1] Ricarda Richter-Dennerlein,[1] Simon E. Tröder,[1] Hans-Georg Sprenger,[1] Pedro M. Quirós,[3] Carlos López-Otín,[3] Elena I. Rugarli,[1,2] and Thomas Langer[1,2,4]

[1]Institute of Genetics and Cologne Excellence Cluster on Cellular Stress Responses in Aging-Associated Diseases and [2]Center for Molecular Medicine, University of Cologne, 50931 Cologne, Germany
[3]Departamento de Bioquímica y Biología Molecular, Facultad de Medicina, Instituto Universitario de Oncología, Universidad de Oviedo, Oviedo 33006, Spain
[4]Max Planck Institute for Biology of Aging, 50931 Cologne, Germany

Proteolytic cleavage of the dynamin-like guanosine triphosphatase OPA1 in mitochondria is emerging as a central regulatory hub that determines mitochondrial morphology under stress and in disease. Stress-induced OPA1 processing by OMA1 triggersmitochondrial fragmentation, which is associated with mitophagy and apoptosis in vitro. Here, we identify OMA1 as a critical regulator of neuronal survival in vivo and demonstrate that stress-induced OPA1 processing by OMA1 promotes neuronal death and neuroinflammatory responses. Using mice lacking prohibitin membrane scaffolds as a model of neurodegeneration, we demonstrate that additional ablation of *Oma1* delays neuronal loss and prolongs lifespan. This is accompanied by the accumulation of fusion-active, long OPA1 forms, which stabilize the mitochondrial genome but do not preserve mitochondrial cristae or respiratory chain supercomplex assembly in prohibitin-depleted neurons. Thus, long OPA1 forms can promote neuronal survival independently of cristae shape, whereas stress-induced OMA1 activation and OPA1 cleavage limit mitochondrial fusion and promote neuronal death.

## Introduction

Mitochondrial dynamics allow the adaptation of mitochondrial activities to varying physiological demands and ensure quality surveillance of mitochondrial function (Friedman and Nunnari, 2014; Mishra and Chan, 2014; Roy et al., 2015). Whereas mitochondrial fusion is considered to be a prosurvival mechanism (Tondera et al., 2009), fission is required for the autophagic removal of damaged mitochondria and occurs early during cell death (Youle and van der Bliek, 2012). Various cellular signals are known to determine the shape of mitochondria (Merrill and Strack, 2014; Mishra et al., 2014; Patten et al., 2014). They modulate the activity of large GTPases of the dynamin superfamily that catalyze fusion and fission of mitochondrial membranes. DRP1 mediates mitochondrial fission, whereas fusion is performed by the concerted action of mitofusins (MFN1 and MFN2) and optic atrophy 1 (OPA1) in the outer and inner mitochondrial membranes (OMM and IMM), respectively.

Acute stress and mitochondrial damage cause fragmentation of the mitochondrial network. This general stress response is often observed under pathologic conditions (Ong et al., 2013; Burté et al., 2015) and involves regulatory steps at both mitochondrial membranes. Mitochondrial depolarization triggers ubiquitin-dependent degradation of mitofusins as well as dephosphorylation and activation of DRP1 at the OMM (Cribbs and Strack, 2007; Cereghetti et al., 2008). At the same time, stress-induced proteolytic cleavage of OPA1 inhibits IMM fusion (Ishihara et al., 2006; Griparic et al., 2007; Song et al., 2007). OPA1 activity is emerging as a central regulatory hub for mitochondrial shape changes and cell survival. Loss of OPA1 impairs mitochondrial fusion, disturbs cristae morphogenesis, and increases the apoptotic sensitivity of cells (Olichon et al., 2003; Cipolat et al., 2004; Meeusen et al., 2006). On the other hand, overexpression of OPA1 protects against apoptotic and ischemic tissue damage and ameliorates phenotypes of mitochondrial disease mouse models (Cipolat et al., 2006; Civiletto et al., 2015; Varanita et al., 2015). OPA1 function is regulated by proteolytic cleavage at sites S1 and S2, which results in the balanced accumulation of noncleaved, long (L-OPA1) and cleaved, short (S-OPA1) OPA1 forms (Ishihara et al., 2006; Griparic et al., 2007). L-OPA1 is sufficient to promote mitochondrial fusion and maintain normal cristae in mouse embryonic fibroblasts (MEFs), whereas S-OPA1 appears to function

Correspondence to Thomas Langer: thomas.langer@uni-koeln.de

Abbreviations used in this paper: BN, blue native; CL, cardiolipin; DG, dentate gyrus; GFAP, glial fibrillary acidic protein; IBA1, ionized calcium binding adaptor molecule 1; IMM, inner mitochondrial membrane; MEF, mouse embryonic fibroblast; mtDNA, mitochondrial DNA; OMM, outer mitochondrial membrane; PHB, prohibitin.



The Rockefeller University Press $30.00
J. Cell Biol. Vol. 212 No. 2 157–166
www.jcb.org/cgi/doi/10.1083/jcb.201507022

in mitochondrial fission (Anand et al., 2014). Two peptidases, OMA1 and the *i*-AAA protease YME1L, cleave OPA1 at S1 and S2, respectively (Song et al., 2007; Ehses et al., 2009; Head et al., 2009; Stiburek et al., 2012; Anand et al., 2014). Whereas OPA1 processing by YME1L is under metabolic control (Mishra et al., 2014), OMA1 is activated upon various stress insults, resulting in the complete degradation of L-OPA1 and mitochondrial fragmentation (Ehses et al., 2009; Baker et al., 2014; Zhang et al., 2014; Quirós et al., 2015). *Oma1*-deficient mice exhibit impaired thermogenesis and diet-induced obesity (Quirós et al., 2012). Moreover, loss of OMA1 in cultured cells was found to protect against apoptosis (Head et al., 2009; Quirós et al., 2012; Jiang et al., 2014; Xiao et al., 2014). However, the general in vivo relevance of stress-induced OPA1 processing by OMA1, and in particular its importance for neuronal survival, is not understood.

Prohibitin membrane scaffolds are required for L-OPA1 stability and cell survival (Kasashima et al., 2008; Merkwirth et al., 2008). They form large ring complexes in the IMM, composed of multiple prohibitin 1 (PHB1) and PHB2 subunits (Tatsuta et al., 2005) constituting functional membrane domains with a defined complement of proteins and lipids (Osman et al., 2009, 2011; Richter-Dennerlein et al., 2014). Loss of PHB2 in MEFs destabilizes L-OPA1 and causes mitochondrial fragmentation, disturbances in mitochondrial ultrastructure, and increased apoptotic sensitivity (Merkwirth et al., 2008). Re-expression of noncleavable L-OPA1 restores these deficiencies, indicating that they are caused by loss of L-OPA1 (Merkwirth et al., 2008).

Forebrain neuron-specific *Phb2*-deficient ($Phb2^{NKO}$) mice display progressive neurodegeneration, culminating in premature death (Merkwirth et al., 2012). Neuronal loss is accompanied by the destabilization of L-OPA1, defects in mitochondrial ultrastructure, loss of mitochondrial DNA (mtDNA), and late-onset mitochondrial dysfunction (Merkwirth et al., 2012). Here, we demonstrate that ablation of *Oma1* prevents loss of L-OPA1, delays neurodegeneration, and extends the lifespan of $Phb2^{NKO}$ mice. Thus, our results establish a crucial role for OMA1 in neuronal survival in vivo.

## Results and discussion

### Genetic loss of *Oma1* extends survival of $Phb2^{NKO}$ mice

We deleted *Oma1* in mice lacking *Phb2* specifically in forebrain neurons ($Phb2^{NKO}$; Merkwirth et al., 2012) by crossing $Phb2^{NKO}$ mice to $Oma1^{ko/ko}$ mice (Quirós et al., 2012). Deletion of *Phb2* resulted in premature death starting at the age of 16 wk, whereas control ($Phb2^{fl/fl}$) and $Oma1^{ko/ko}$ mice showed normal lifespans (Fig. 1 A; Quirós et al., 2012). Notably, additional deletion of *Oma1* significantly extended the median survival of $Phb2^{NKO}$ mice by 25% (Fig. 1 A), indicating that OMA1 limits neuronal survival in $Phb2^{NKO}$ mice.

We therefore analyzed brain morphology and brain weight in 18-wk-old $Phb2^{NKO}$, $Oma1^{ko/ko}$, and $Phb2^{NKO}Oma1^{ko/ko}$ mice (Fig. 1, B and C). Although $Oma1^{ko/ko}$ brains appeared morphologically normal, extensive forebrain atrophy was evident in $Phb2^{NKO}$ mice (Fig. 1 B). In contrast, brains of $Phb2^{NKO}Oma1^{ko/ko}$ mice were morphologically indistinguishable from those of controls (Fig. 1 B). Consistently, loss of *Oma1* significantly restored brain weights of $Phb2^{NKO}$ mice (Fig. 1 C). Semithin sections of the hippocampal dentate gyrus (DG) from 14- and 18-wk-old animals further revealed progressive neurodegeneration in $Phb2^{NKO}$ mice (Fig. 1, D and E). Notably, deletion of *Oma1* fully suppressed neuronal loss in the hippocampus of 14-wk-old $Phb2^{NKO}$ mice (Fig. 1 E); however, almost all neurons contained vacuolated structures (Fig. 1 E). Mild neuronal degeneration became apparent only in 18-wk-old $Phb2^{NKO}Oma1^{ko/ko}$ mice (Fig. 1, D and E). We therefore conclude that deletion of *Oma1* delays the onset of neurodegeneration in $Phb2^{NKO}$ mice and increases their lifespan.

### *Oma1* deletion in $Phb2^{NKO}$ mice delays neuroinflammation

Neuroinflammation, characterized by the activation of microglia and astrocytes, is an early feature of neurodegenerative processes (Khandelwal et al., 2011). Neuronal loss in $Phb2^{NKO}$ mice is accompanied by up-regulation of glial fibrillary acidic protein (GFAP) in astrocytes, already apparent at 6 wk of age (Merkwirth et al., 2012). Immunohistochemical and immunoblot analyses of the hippocampus of 14-wk-old $Phb2^{NKO}$ mice revealed accumulation of GFAP and ionized calcium binding adaptor molecule 1 (IBA1), indicating astrogliosis and activated microglia, respectively (Fig. 2, A and B). In contrast, GFAP levels in hippocampal lysates, as well as GFAP and IBA1 immunoreactivities in the hippocampus of age-matched $Phb2^{NKO}Oma1^{ko/ko}$ mice, were similar to those of control mice (Fig. 2, A and B). GFAP protein levels and GFAP staining moderately increased in 18-wk-old $Phb2^{NKO}Oma1^{ko/ko}$ mice, suggesting that the neuroinflammatory response is retarded but not entirely suppressed (Fig. S1, B and C). Thus, loss of *Oma1* prolongs neuronal survival and delays astrogliosis and the activation of microglia in the absence of PHB2.

To assess the expression of proinflammatory cytokines, we isolated total RNA from the hippocampus of 14-wk-old $Phb2^{NKO}$, $Oma1^{ko/ko}$, $Phb2^{NKO}Oma1^{ko/ko}$, and control mice and analyzed mRNA levels by real-time PCR (Fig. 2 C). Whereas ablation of *Oma1* did not affect cytokine expression, the relative expression of *IL-1β*, *IL-6*, and *TNF* was increased in $Phb2^{NKO}$ mice (Fig. 2 C). Remarkably, this response was completely abrogated in $Phb2^{NKO}Oma1^{ko/ko}$ mice (Fig. 2 C). Together, these experiments reveal that OMA1 triggers neuronal loss and early inflammatory responses in the absence of PHB2.

### *Oma1* deletion protects *Phb2*-deficient cells against apoptosis

Loss of OMA1 protects cultured cells against apoptosis (Head et al., 2009; Quirós et al., 2012; Jiang et al., 2014; Xiao et al., 2014). We have previously described that apoptosis contributes to neuronal loss in $Phb2^{NKO}$ mice, but have detected only a limited number of TUNEL-positive neurons (Merkwirth et al., 2012). Consistently, immunoblot analysis did not provide evidence of apoptotic or necrotic cell death or of altered autophagy in hippocampal lysates (Fig. S1 D), which is likely caused by rapid loss of *Phb2*-deficient neurons. We therefore used *Phb2*-deficient MEFs, which exhibit increased apoptotic sensitivity (Merkwirth et al., 2012), to investigate whether *Oma1* deletion restores their apoptotic resistance. We depleted PHB2 from control (wild-type) and $Oma1^{-/-}$ MEFs and induced apoptosis by $H_2O_2$ treatment (Fig. 3, A and B). Poly(ADP ribose) polymerase and caspase-3 cleavage was undetectable in $Oma1^{-/-}$ cells lacking prohibitins, whereas apoptotic marker proteins accumulated in *Phb2*-deficient control cells (Fig. 3 A).

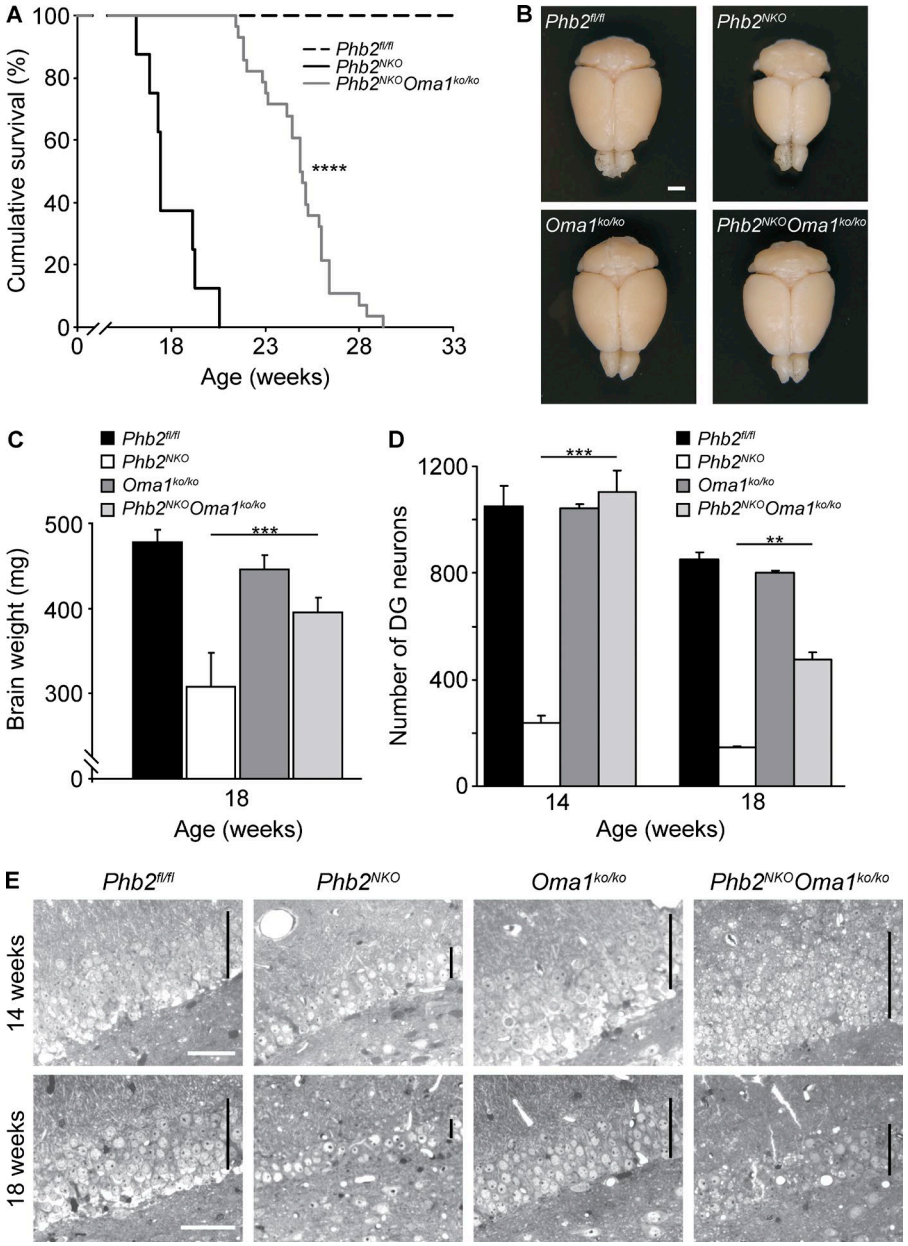


Figure 1. ***Oma1* deletion in *Phb2*$^{NKO}$ mice is neuroprotective.** (A) Loss of OMA1 prolongs the lifespan of *Phb2*$^{NKO}$ mice. Kaplan–Meier survival plot of *Phb2*$^{NKO}$ ($n$ = 15), *Phb2*$^{NKO}$*Oma1*$^{ko/ko}$ ($n$ = 28), and *Phb2*$^{fl/fl}$ animals ($n$ = 30). ****, P < 0.0001. (B) Deletion of *Oma1* in *Phb2*$^{NKO}$ mice prevents brain atrophy. Representative photographs of brains isolated from 18-wk-old mice. Bar, 2 mm. (C) Brain weights were monitored at 18 wk of age (*Phb2*$^{fl/fl}$, $n$ = 10; *Phb2*$^{NKO}$, $n$ = 7; *Oma1*$^{ko/ko}$, $n$ = 9; *Phb2*$^{NKO}$*Oma1*$^{ko/ko}$, $n$ = 14). ***, P < 0.001. Error bars indicate SD. (D) *Oma1* ablation in *Phb2*$^{NKO}$ mice improves neuronal survival. Number of DG neurons in 14- and 18-wk-old mice of the indicated genotypes ($n$ = 3). **, P < 0.01; ***, P < 0.001. Error bars indicate SD. (E) Coronal semithin sections of the hippocampal DG from 14- and 18-wk-old mice. Black vertical bars show the thickness of the neuronal layers. Bars, 50 µm.

Consistently, FACS analysis revealed that depletion of prohibitins did not affect the viability of $H_2O_2$-treated *Oma1*$^{-/-}$ cells, whereas we observed reduced viability of *Phb2*-deficient control MEFs upon $H_2O_2$-induced apoptosis (Fig. 3 B). Thus, *Oma1* deletion in cells lacking prohibitins protects against apoptosis induced by $H_2O_2$. To further define its role in cell death pathways, we analyzed necroptotic sensitivity of MEFs lacking OMA1. Cells treated with TNF, cycloheximide, and Z-VAD-FMK undergo necroptosis, which can be inhibited by necrostatin 1 or deletion of *Ripk3* (Polykratis et al., 2014). Deletion of *Oma1* did not improve cell viability upon induction of necroptosis, whereas *Ripk3*-deficient cells were fully viable (Figs. 3 C and S1 E). In contrast, loss of *Oma1* conferred resistance to apoptosis induced by TNF and cycloheximide only (Fig. 3 C). Thus, *Oma1* deletion in cultured MEFs protects against apoptosis but not against necroptosis, suggesting that loss of *Oma1* in *Phb2*$^{NKO}$ mice prevents apoptotic death, resulting in extended neuronal survival.

### OMA1 cleaves neuronal L-OPA1 in *Phb2*$^{NKO}$ mice

We therefore turned our attention to the anti-apoptotic OMA1 substrate OPA1 (Olichon et al., 2003; Frezza et al., 2006). OPA1 splice variant 1, the predominantly expressed OPA1 isoform in the brain (Akepati et al., 2008), gives rise to L-OPA1, which is processed to S-OPA1 by OMA1. Neurons lacking prohibitins display selective loss of L-OPA1 and accumulation of S-OPA1, indicating OMA1 activation. Deletion of *Oma1* in *Phb2*$^{NKO}$ mice resulted in L-OPA1 stabilization in hippocampal lysates from 14- and 18-wk-old mice (Fig. 4, A and B). Residual S-OPA1 likely resulted from YME1L-mediated OPA1 cleavage at S2. Another OMA1 substrate under stress conditions, C11orf83 (Desmurs et al., 2015), did not accumulate upon loss of OMA1 (Fig. S2 A). Hence, we conclude that neuronal ablation of *Phb2* activates OMA1, triggering stress-induced processing of L-OPA1.

L-OPA1 is sufficient to mediate fusion and preserve cristae morphogenesis, rendering cultured cells resistant against

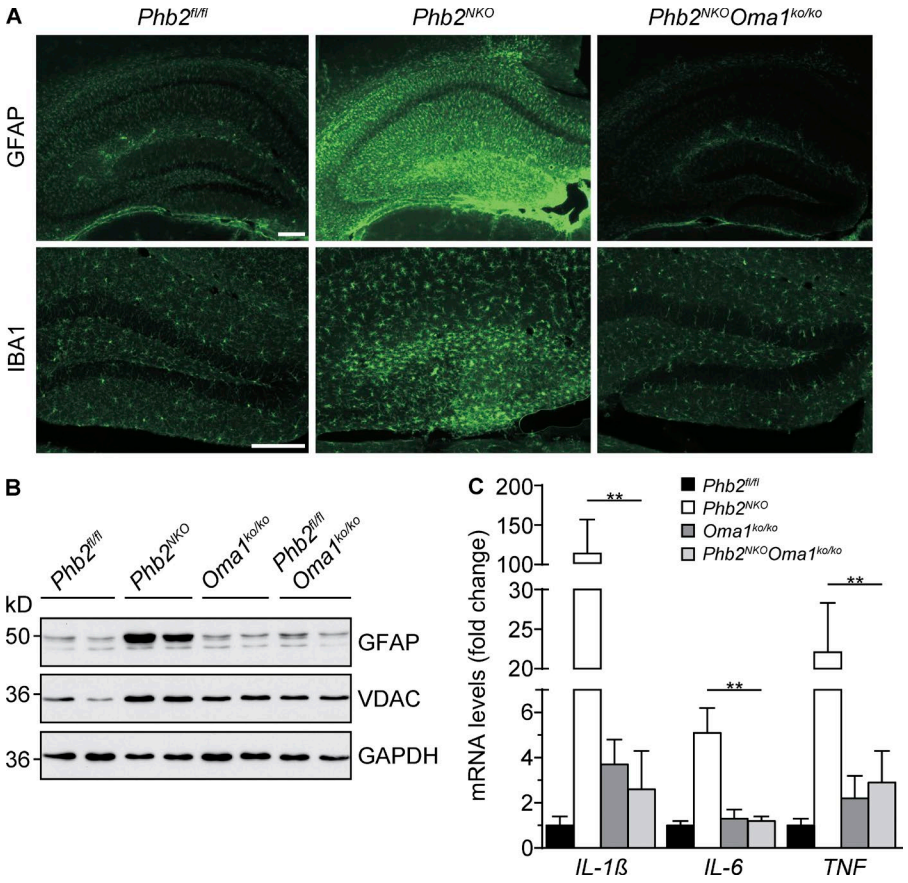


Figure 2. ***Oma1* deletion in *Phb2*$^{NKO}$ mice prevents neuroinflammation.** (A) Reactive astrogliosis and activation of microglia in *Phb2*$^{NKO}$ mice is blocked by deletion of *Oma1*. Immunohistochemical staining of coronal sections across the hippocampal region from 14-wk-old mice using GFAP- and IBA1-specific antibodies. Bars, 200 µm. (B) Immunoblot analysis of hippocampal lysates from 14-wk-old mice. GAPDH was used as a loading control. (C) mRNA levels of proinflammatory cytokines in *Phb2*$^{NKO}$ mice are restored upon deletion of *Oma1*. Total RNA was isolated from the hippocampus of 14-wk-old mice and subjected to quantitative real-time PCR analysis ($n$ = 3). Transcript levels were normalized to *Gapdh* mRNA levels. **, P < 0.01. Error bars indicate SD.

apoptosis (Anand et al., 2014). We therefore assessed the ultrastructure of mitochondria in DG neurons of *Phb2*$^{NKO}$, *Oma1*$^{ko/ko}$, and *Phb2*$^{NKO}$*Oma1*$^{ko/ko}$ mice by transmission electron microscopy (Fig. 4 C). The ultrastructure of neuronal mitochondria was grossly unaffected in the absence of OMA1 (Fig. 4 C). In contrast, we observed aberrant neuronal mitochondria lacking cristae in *Phb2*$^{NKO}$ mice already at 6 wk of age (Fig. 4 C). Surprisingly, ablation of *Oma1* in these mice did not restore cristae, but mitochondria were considerably enlarged (Fig. 4 C). Quantification of mitochondrial surface area confirmed that *Phb2*$^{NKO}$*Oma1*$^{ko/ko}$ mice contained substantially larger mitochondria, whereas mitochondrial size was altered in neither *Phb2*$^{NKO}$ nor *Oma1*$^{ko/ko}$ mice (Fig. S2, B and C). In addition, we performed immunohistochemistry on hippocampal sections from 18-wk-old mice using TOMM20-specific antibodies to visualize mitochondrial morphology (Fig. S2 D). Mitochondria appeared normal in *Phb2*$^{NKO}$, *Oma1*$^{ko/ko}$, and *Phb2*$^{fl/fl}$ mice but enlarged and swollen in *Phb2*$^{NKO}$*Oma1*$^{ko/ko}$ mice, reminiscent of mitochondrial morphological changes observed in *Drp1*-deficient hippocampal neurons (Shields et al., 2015; Oettinghaus et al., 2016).

OPA1 oligomerization contributes to the maintenance of cristae shape (Frezza et al., 2006; Patten et al., 2014). In accordance with the observed ultrastructural defects, analysis of OPA1 assembly by chemical cross-linking revealed significantly reduced OPA1 complex levels in hippocampal mitochondria isolated from 18-wk-old *Phb2*$^{NKO}$ and *Phb2*$^{NKO}$*Oma1*$^{ko/ko}$ mice (Fig. 4 D).

Thus, L-OPA1 stabilization in OMA1-deficient *Phb2*$^{NKO}$ mice does not restore OPA1 oligomerization and mitochondrial ultrastructure. The prolonged survival of PHB2-deficient neurons upon ablation of *Oma1* can therefore not be explained by effects of L-OPA1 on cristae morphogenesis. Rather, our results indicate that stabilization of L-OPA1 and mitochondrial fusion ensures neuronal survival in the absence of PHB2, demonstrating a crucial role of OMA1 in neuronal survival in vivo. In light of our observations, it is conceivable that the protective effect of OPA1 overexpression in various mitochondrial disease mouse models (Civiletto et al., 2015; Varanita et al., 2015) can be attributed to L-OPA1 only, which drives fusion and can support cell survival independently of cristae morphogenesis.

Loss of *Oma1* not only stabilizes L-OPA1 but also impairs the formation of S-OPA1. S-OPA1 was proposed to stimulate fission and induce mitochondrial fragmentation (Anand et al., 2014). Thus, unopposed fusion events may explain the formation of giant mitochondria that were already observed in young OMA1-deficient *Phb2*$^{NKO}$ neurons. Notably, we also observed moderately reduced accumulation of some components of the mitochondrial fission machinery in hippocampal lysates of *Phb2*$^{NKO}$*Oma1*$^{ko/ko}$ mice (Fig. S2 E).

## Ablation of *Oma1* in *Phb2*$^{NKO}$ mice restores mtDNA levels but does not preserve respiratory function

*Oma1* deletion in *Phb2*$^{NKO}$ mice prolongs neuronal survival and extends lifespan, but *Phb2*$^{NKO}$*Oma1*$^{ko/ko}$ mice still display reduced survival. We thus reasoned that L-OPA1–independent neuronal functions of PHB2 limit the lifespan of *Phb2*$^{NKO}$*Oma1*$^{ko/ko}$ mice. We have previously described respiratory defects in *Phb2*$^{NKO}$ mice at late stages (Merkwirth et al., 2012). To examine whether OMA1 affects mitochondrial respiratory function in prohibitin-deficient neurons, we monitored

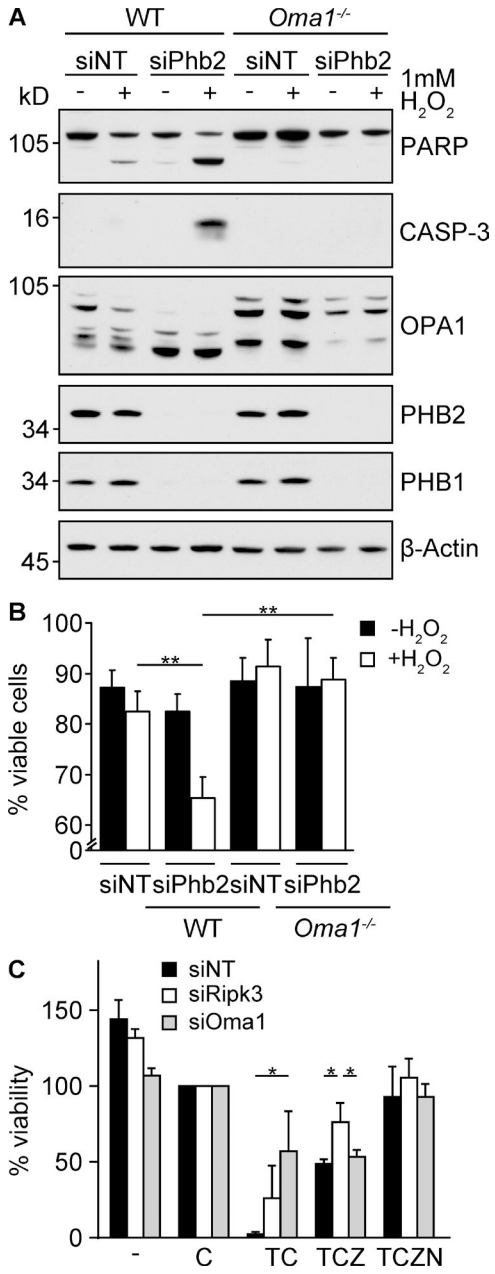


Figure 3. ***Oma1* deletion restores apoptotic resistance of *Phb2*-deficient cells but does not protect against TNF-induced necroptosis.** (A and B) *Oma1* deletion protects *Phb2*-deficient MEFs against $H_2O_2$-induced apoptosis. siRNA-treated wild-type (WT) and *Oma1*$^{-/-}$ cells were exposed to 1 mM $H_2O_2$ for 7 h. (A) Analysis of the accumulation of apoptotic marker proteins by immunoblotting. β-Actin was used as a loading control. (B) Flow cytometry analysis of viable cells (7-AAD–negative, Annexin V–negative; $n = 3$). **, $P < 0.01$. Error bars indicate SD. (C) *Oma1* deletion does not confer necroptotic resistance. Cell viability of *Oma1*-deficient MEFs was analyzed upon induction of necroptosis. –, DMSO; C, cycloheximide; T, TNF; Z, Z-VAD-FMK; N, necrostatin-1. *, $P < 0.05$. Error bars indicate SD.

the assembly of respiratory chain complexes in hippocampal mitochondria isolated from 18-wk-old *Phb2*$^{NKO}$, *Oma1*$^{ko/ko}$, and *Phb2*$^{NKO}$*Oma1*$^{ko/ko}$ mice by blue native (BN)-PAGE (Fig. 5, A and B). Supercomplexes composed of complexes I, III, and IV; complexes I and III; and complexes III and IV were observed in *Oma1*$^{ko/ko}$ and *Phb2*$^{fl/fl}$ control mice, which were present at markedly reduced levels in hippocampal mitochondria of *Phb2*$^{NKO}$ mice (Fig. 5 A). Additional deletion of *Oma1* did not restore the formation of these supercomplexes (Fig. 5 A). Consistently, enzymatic in-gel activity assays in hippocampal mitochondria revealed decreased complex I and IV activities in both *Phb2*$^{NKO}$ and *Phb2*$^{NKO}$*Oma1*$^{ko/ko}$ mice but not in *Oma1*$^{ko/ko}$ mice (Fig. 5 B). Therefore, deletion of *Oma1* does not restore respiratory function in *Phb2*$^{NKO}$ mice.

Several scenarios, which are not mutually exclusive, can be envisioned to explain respiratory deficiencies in *Phb2*$^{NKO}$*Oma1*$^{ko/ko}$ mice: loss of PHB2 may affect mtDNA stability, synthesis of mitochondrial encoded respiratory chain subunits, or assembly of the respiratory chain, irrespective of the presence of OMA1. We therefore monitored mtDNA levels in the hippocampus and striatum of 18-wk-old *Phb2*$^{NKO}$, *Oma1*$^{ko/ko}$, and *Phb2*$^{NKO}$*Oma1*$^{ko/ko}$ mice by quantitative real-time PCR (Figs. 5 C and S3 A). In agreement with our previous findings (Merkwirth et al., 2012), we observed a decrease of mtDNA levels to ∼40% in *Phb2*$^{NKO}$ mice (Figs. 5 C and S3 A). Conversely, mtDNA levels were slightly increased in *Oma1*$^{ko/ko}$ mice and completely restored in *Phb2*$^{NKO}$*Oma1*$^{ko/ko}$ mice (Figs. 5 C and S3 A). Thus, mtDNA levels can be maintained in neurons lacking PHB2 by stabilizing L-OPA1.

To explain respiratory deficiencies in *Phb2*$^{NKO}$*Oma1*$^{ko/ko}$ mice, we next assessed mitochondrial protein synthesis in the cerebral cortex of 14-wk-old mice (Fig. S3, B and C). As previously shown in prohibitin-depleted cells in vitro (He et al., 2012), we observed reduced mitochondrial protein synthesis in *Phb2*$^{NKO}$ mice, which was not restored by deletion of *Oma1* (Fig. S3, B and C). However, impaired translation does not cause respiratory deficiencies in *Phb2*$^{NKO}$*Oma1*$^{ko/ko}$ mice, as respiratory chain complex subunits accumulated at similar steady-state levels in hippocampal mitochondria irrespective of the presence or absence of PHB2 and OMA1 (Fig. 5 D). These observations thus indicate that prohibitins affect the assembly of respiratory chain supercomplexes in a posttranslational manner, resulting in respiratory defects in PHB2-deficient neurons.

We have previously observed decreased levels and changes in the acyl chain composition of cardiolipin (CL) in mitochondrial membranes lacking PHB2, suggesting a role of PHB membrane scaffolds in CL remodeling (Richter-Dennerlein et al., 2014). CL stabilizes respiratory chain supercomplexes and maintains cristae morphogenesis (Pfeiffer et al., 2003; Schlame, 2013). An altered membrane lipid composition in the absence of PHB2 may thus affect mitochondrial cristae structure and the assembly of respiratory chain supercomplexes, irrespective of L-OPA1 stability and the presence of OMA1. Consistently, loss of DNAJC19, regulating CL metabolism and interacting with PHB complexes, disturbs the ultrastructure of mitochondria, which is not restored upon additional ablation of *Oma1* (Richter-Dennerlein et al., 2014). However, to clarify the role of PHB membrane scaffolds for mitochondrial shape and function in neurons, it is necessary to define how loss of PHB2 affects the lipid composition of mitochondrial membranes specifically in affected neurons before other scenarios can be excluded. Regardless, the analysis of OMA1-deficient *Phb2*$^{NKO}$ mice unravels essential, L-OPA1–independent functions of PHB membrane scaffolds in mitochondria. These functions likely limit the lifespan of *Phb2*$^{NKO}$*Oma1*$^{ko/ko}$ mice and may explain the embryonic lethality of PHB2-deficient mice lacking OMA1 (Fig. S1 A).

Together, our results identified OMA1 as a critical regulator of neuronal survival in vivo and revealed critical roles of OMA1-mediated OPA1 processing in neurodegeneration. We demonstrate that loss of PHB membrane scaffolds

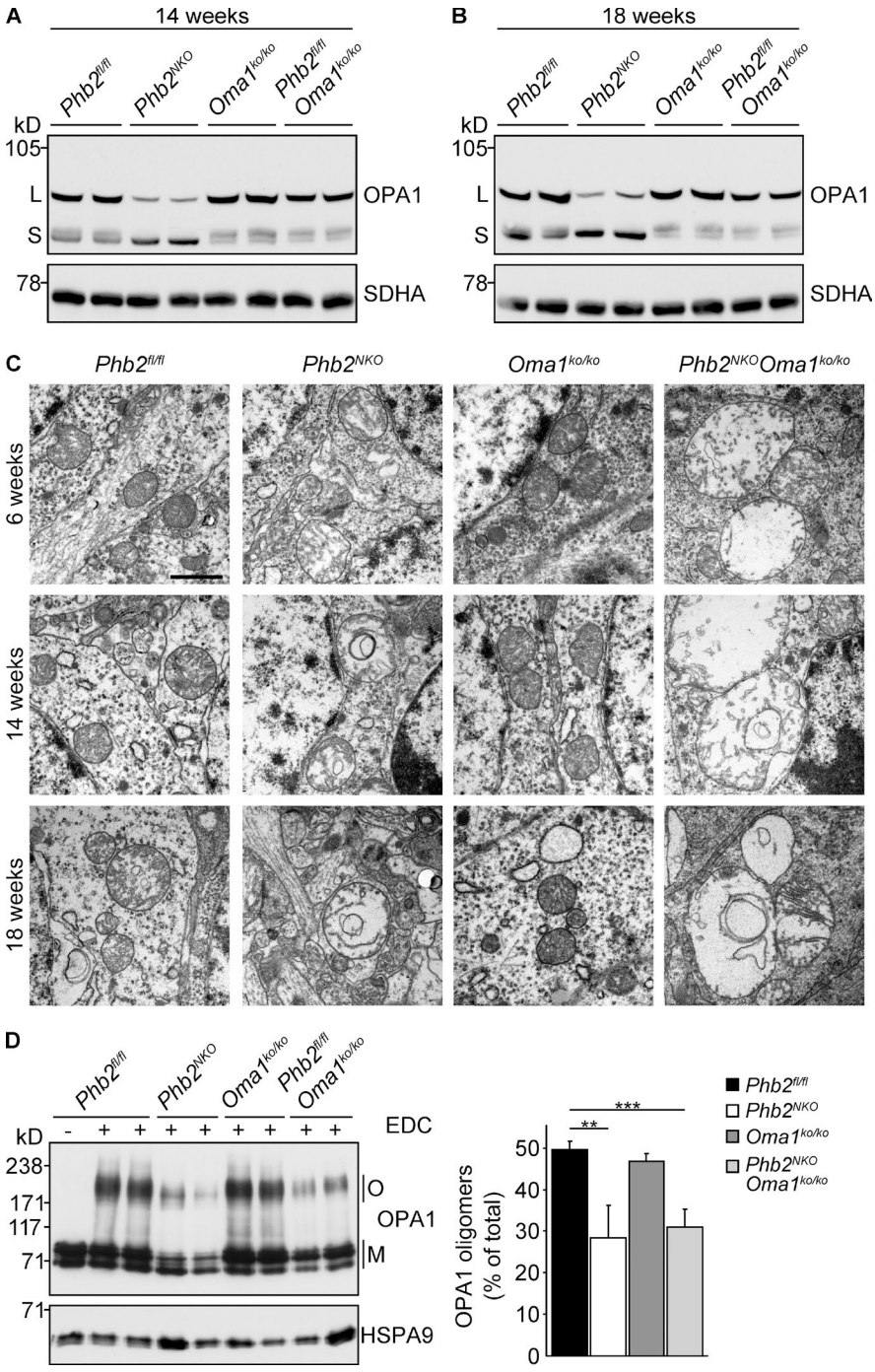


Figure 4. **OMA1-mediated OPA1 processing in *Phb2*$^{NKO}$ mice and mitochondrial ultrastructure.** (A and B) L-OPA1 is stabilized upon deletion of *Oma1* in *Phb2*$^{NKO}$ mice. Hippocampal lysates isolated from 14-wk-old (A) or 18-wk-old (B) mice were analyzed by immunoblotting. SDHA was used as a loading control. (C) Hippocampal DG neurons of *Phb2*$^{NKO}$*Oma1*$^{ko/ko}$ mice contain large, swollen mitochondria lacking cristae. Analysis of mitochondrial ultrastructure in DG neurons of 6-, 14-, and 18-wk-old mice by transmission electron microscopy. Bar, 1.2 µm. (D) Impaired OPA1 oligomerization in *Phb2*$^{NKO}$ and *Phb2*$^{NKO}$*Oma1*$^{ko/ko}$ mitochondria. OPA1 complex formation was analyzed in hippocampal mitochondria isolated from 18-wk-old mice of the indicated genotypes cross-linked with 1 mM EDC. OPA1 oligomers were visualized by immunoblotting (left panel), and complex levels were quantified using ImageJ (right panel; $n = 4$). HSPA9 was used as a loading control. O, oligomers; M, monomers. **, $P \leq 0.01$; ***, $P \leq 0.001$.

activates OMA1, resulting in L-OPA1 degradation and neuronal death. Ablation of *Oma1* in PHB2-deficient neurons stabilizes fusion-active L-OPA1, which supports neuronal survival by preventing apoptosis, independent of its effects on cristae morphogenesis.

## Materials and methods

### Mice

Neuron-specific *Phb2*-deficient mice (*Phb2*$^{NKO}$) on a C57BL/6N background were generated by crossing mice in which exons 3 and 4 of the *Phb2* gene were flanked by loxP sites (*Phb2*$^{fl/fl}$) with mice expressing Cre recombinase under control of the postnatally expressed *CaMKIIα* promoter, allowing recombination specifically in forebrain neurons (Merkwirth et al., 2012). *Oma1*$^{-/-}$ mice on a C57BL/6N background were generated by deleting exon 2 of the *Oma1* gene (Quirós et al., 2012). For the present study, *Phb2*$^{NKO}$ and *Phb2*$^{NKO}$*Oma1*$^{ko/ko}$ mice were obtained by crossing *Phb2*$^{fl/fl}$ *Oma1*$^{ko/WT}$ *CaMKIIα-Cre*$^{tg/WT}$ and *Phb2*$^{fl/fl}$ *Oma1*$^{ko/WT}$ mice. Care of all animals was within institutional animal care committee guidelines, and all procedures were approved by local government authorities (Bezirksregierung Köln) and were in accordance with National Institutes of Health guidelines.

### Neuropathology and ultrastructural analysis

Mice were anesthetized and perfused with 2% glutaraldehyde in PBS. Brains were removed and kept in 0.12 M phosphate buffer/2% glutaraldehyde. After treatment with osmium tetroxide, brains were embedded

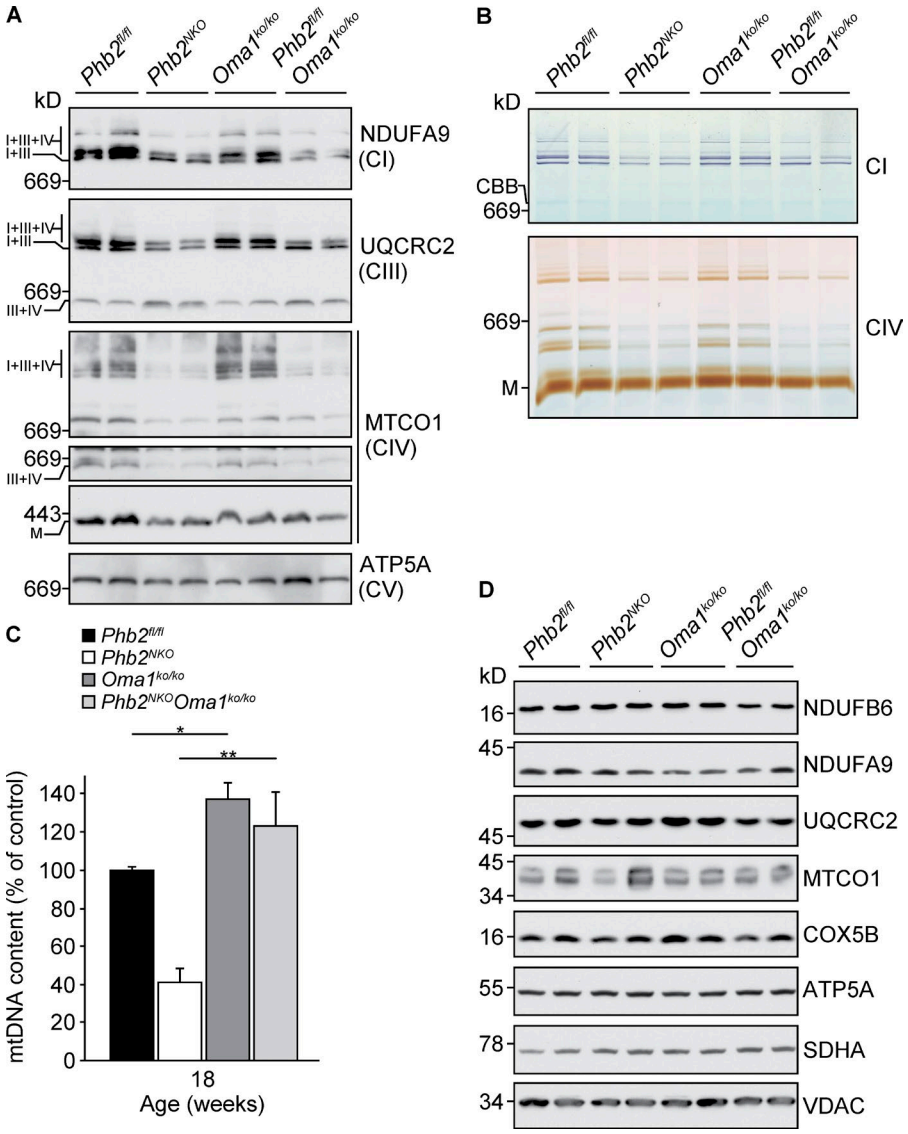


Figure 5. **Stabilization of mtDNA in *Phb2*$^{NKO}$ mice upon *Oma1* deletion.** (A) Assembly of respiratory chain supercomplexes is impaired in *Phb2*$^{NKO}$ and *Phb2*$^{NKO}$*Oma1*$^{ko/ko}$ mice. Digitonin-solubilized hippocampal mitochondria isolated from 18-wk-old mice were analyzed by BN-PAGE and immunoblotting using the indicated antibodies. I, complex I; III, complex III; IV, complex IV; M, monomer. (B) Relative activities of complexes I and IV are decreased in *Phb2*$^{NKO}$ and *Phb2*$^{NKO}$*Oma1*$^{ko/ko}$ mice. Mitochondria isolated from the hippocampus of 18-wk-old mice were subjected to BN-PAGE, and gels were incubated in complex I (CI)- or complex IV (CIV)-specific substrate solutions. M, monomeric CIV. (C) Relative mtDNA levels in the hippocampus of 18-wk-old mice. Total DNA was isolated from the hippocampus of mice of the indicated genotype and analyzed by quantitative real-time PCR analysis using mtDNA- and nuclear DNA–specific primers ($n$ = 3). *, P≤ 0.05; **, P < 0.01. Error bars indicate SD. (D) Steady-state levels of respiratory chain complex subunits in *Phb2*$^{NKO}$ and *Phb2*$^{NKO}$*Oma1*$^{ko/ko}$ mice. Immunoblot analysis of hippocampal mitochondria isolated from 18-wk-old mice using the indicated antibodies.

in Epon. Semithin (1 µm) coronal sections were cut from hippocampus, mounted with Eukitt, and observed using an Axio-Imager M2 microscope equipped with an AxioCamICc1 camera (Carl Zeiss). Images were acquired at 20× (Plan-Apochromat 20×/0.8) using AxioVision software (version 4.8.2.0; Carl Zeiss). The number of DG neurons was quantified by counting neuronal cell bodies in the whole DG area of the hippocampus. For EM analyses, ultrathin sections (70 nm) were cut and stained with uranium acetate and lead citrate (Almajan et al., 2012). Images were acquired using a transmission electron microscope at 13,500× (CM10; Philips) and an acceleration voltage of 80 kV using a camera (Gatan). Mitochondrial surface area was calculated from mitochondria imaged by transmission electron microscopy using ImageJ software (6 wk: *Phb2*$^{fl/fl}$, $n$ = 20; *Phb2*$^{NKO}$, $n$ = 31; *Oma1*$^{ko/ko}$, $n$ = 17; and *Phb2*$^{NKO}$*Oma1*$^{ko/ko}$, $n$ = 40; 14 wk: *Phb2*$^{fl/fl}$, $n$ = 20; *Phb2*$^{NKO}$, $n$ = 36; *Oma1*$^{ko/ko}$, $n$ = 26; and *Phb2*$^{NKO}$*Oma1*$^{ko/ko}$, $n$ = 43).

### Immunohistochemistry

Animals were anesthetized and perfused intracardially with 4% paraformaldehyde. Brains were removed and conserved in 0.12 M phosphate buffer. Immunohistochemical analyses were performed on 30-µm-thick coronal free-floating sections. The following antibodies were used in this study: mouse anti-GFAP (1:350; MS-280-P0; Thermo Fisher Scientific), rabbit anti-IBA1 (1:3,000; 019-19741; Wako), and rabbit anti-TOMM20 (1:1,000; sc-11415; Santa Cruz Biotechnology, Inc.). Coronal free-floating sections were incubated for 30 min in 4% sucrose/PBS and for another 30 min in methanol. Afterward, sections were permeabilized and blocked in 10% goat serum and 0.4% Triton X-100 for 1 h. Incubation with the primary antibodies was performed overnight in 5% goat serum and 0.4% Triton X-100. After rinsing with PBS, secondary antibodies (Alexa Fluor anti–mouse 488, anti–rabbit 488, and anti–rabbit 568; Invitrogen) diluted in 5% goat serum were applied for 2 h, and sections were mounted with Fluorsave. Images were acquired using an Axio-Imager M2 microscope equipped with an AxioCamICc1 camera (Carl Zeiss), 5× (EC Plan-Neofluar 5×/0.16 Ph 1), or 10× (EC Plan-Neofluar 10×/0.3 Ph 1) objective lenses and AxioVision software for GFAP and IBA1 stains as well as an UltraVIEW VoX spinning disc confocal microscope (PerkinElmer) on a TiE microscope (Nikon) equipped with a 60× objective lens (Plan-Apo Tirf 60×/1.49 oil), a camera (AMCCD C9100-50; CamLink), and Volocity software (PerkinElmer) for TOMM20 immunohistochemistry. Analyses were performed on at least three mice per genotype.

### Determination of cytokine mRNA levels by RT-PCR

Total RNA was isolated from brain tissues using the NucleoSpin RNA kit (Macherey-Nagel). cDNA was synthesized with the

SuperScript III First-Strand Synthesis System kit (Invitrogen). Quantitative real-time PCR analysis was performed with the ABI PRISM 7000 sequence detection system using Power SYBR Green PCR Master Mix (Applied Biosystems). Transcript levels were normalized to *Gapdh* expression.

### Isolation of mitochondria

Mitochondria-enriched membrane fractions were isolated by differential centrifugation. Brain tissues were dissected from mice, cut into small pieces, and homogenized in an appropriate amount of isolation buffer (20 mM Hepes, pH 7.4, 220 mM D-mannitol, 70 mM sucrose, 2 mM EGTA, and 0.1% BSA [wt/vol]) at 1,000 rpm in a motor-driven dounce homogenizer (Braun). The crude homogenate was centrifuged at 1,000 *g* for 10 min to pellet nuclei and unbroken cells, and the pellet obtained was homogenized again. Subsequently, mitochondria were collected by centrifugation of the supernatants (8,000 *g* for 10 min) and resuspended in freezing buffer (10 mM Hepes-KOH, pH 7.4, and 500 mM sucrose). Protein concentration was determined using Bradford protein assays, and mitochondria were kept frozen until further use.

### Immunoblotting

Brain tissues were dissected and homogenized using a Polytron homogenizer (IKA Werke) in ice-cold lysis buffer (50 mM Hepes/KOH, pH 7.4, 10 mM EDTA, 50 mM NaCl, 100 mM NaF, 1% Triton X-100, and 0.1% SDS supplemented with 20 µg/ml aprotinin, 2 mM benzamidine, 10 mM sodium orthovanadate, and complete protease inhibitor cocktail mix; Roche). Cells were harvested by scraping and lysed in lysis buffer (50 mM Tris-HCl, pH 7.4, 1 mM EDTA, 150 mM NaCl, 1% Triton X-100, 0.1% SDS, 0.5% sodium deoxycholate, and complete protease inhibitor cocktail mix). 50–100 µg total protein was separated by SDS-PAGE, transferred to nitrocellulose membranes, and subjected to immunoblotting using the following antibodies: mouse anti-OPA1 (612606; BD Biosciences), mouse anti-VDAC/Porin (529536; Calbiochem), rabbit anti-GFAP (Z0334; Dako), mouse anti-GAPDH (sc-32233; Santa Cruz Biotechnology, Inc.), mouse anti-SDHA (459200; Invitrogen), rabbit anti-HSPA9 (14887-1-AP; ProteinTech), rabbit anti–poly(ADP ribose) polymerase (9542; Cell Signaling), rabbit anti–cleaved caspase-3 (9661; Cell Signaling), rabbit anti-PHB2 (611802; BioLegend), rabbit anti-PHB1 (603102; BioLegend), mouse anti–β-actin (A5441; Sigma-Aldrich), mouse anti-Spectrin (MAB1622; Merck Millipore), mouse anti-p62 (H00008878-M01; Abnova), rabbit anti-LC3 (PM036; MBL), rabbit anti-RIPK3 (ADI-905-242; Enzo), rabbit anti-MFN2 (ab50838; Abcam), mouse anti-DRP1 (611112; BD Biosciences), rabbit anti–P-DRP1 (S616; 3455; Cell Signaling), rabbit anti-MID49 (16413-1-AP; ProteinTech), rabbit anti-MID51 (20164-1-AP; ProteinTech), rabbit anti-FIS1 (10956-1-AP; ProteinTech), rabbit anti-MFF (17090-1-AP; ProteinTech), mouse anti-NDUFA9 (459100; Invitrogen), mouse anti-UQCRC2 (459220; Invitrogen), mouse anti-MTCO1 (459600; Invitrogen), mouse anti-ATP5A (459240; Invitrogen), mouse anti-NDU FB6 (A21359; Invitrogen), mouse anti-COX5b (459110; Invitrogen), and mouse anti-C11orf83 (Ab-1342-YOM; Primm).

### Cell culture

MEFs were cultured at 37°C (humidified, 5% $CO_2$ [vol/vol]) in DMEM-GlutaMAX (Thermo Fisher Scientific) supplemented with 10% (vol/vol) FBS, 1 mM sodium pyruvate, and nonessential amino acids. siRNA transfections using Lipofectamine RNAiMAX (Thermo Fisher Scientific) were performed according to the manufacturer's protocol. Cells were grown for 72 h and used for further experiments. The efficiency of down-regulation was assessed by immunoblotting.

### Cell death analysis

MEFs were treated with 1 mM $H_2O_2$ for 7 h to induce apoptosis. Apoptotic cell death was assessed by Annexin V and 7-AAD staining, and cells were analyzed by flow cytometry (FACS Aria III; BD Biosciences). The accumulation of apoptotic marker proteins was analyzed by immunoblotting. To induce necroptosis, MEFs were pretreated with 40 µM necrostatin 1 and/or 50 µM Z-VAD-FMK for 2 h and then treated with 20 ng/ml hTNFα, 10 µg/ml cycloheximide, 40 µM necrostatin-1, and/or 50 µM Z-VAD-FMK for 8 h. Afterward, cell viability was measured using CellTiter-Glo luminescent cell viability assay (Promega) according to the manufacturer's instructions.

### Analysis of OPA1 oligomerization

OPA1 oligomerization was analyzed by cross-linking (Patten et al., 2014) and BN-PAGE. For cross-linking, isolated hippocampal mitochondria were suspended in freezing buffer (0.5 M sucrose and 10 mM Hepes, pH 7.4) at 0.5 µg mitochondrial protein/µl. 1 mM EDC (Thermo Fisher Scientific) was added for 30 min at RT, and the reaction was quenched with 0.1% β-mercaptoethanol for 15 min. Samples were analyzed by immunoblotting.

### BN-PAGE

Hippocampal mitochondria (100 µg) were solubilized in 50 mM NaCl, 5 mM 6-aminohexanoic acid, 50 mM imidazole/HCl, pH 7, 10% (vol/vol) glycerol, and 50 mM KPi-buffer, pH 7.4, supplemented with detergent (8 g digitonin/g protein). After extraction for 30 min and a clarifying spin at 16,100 *g* for 30 min, samples were separated by 3%–13% BN-PAGE. For in-gel activity staining, native gels were incubated with substrates specific for complex I (2 mM Tris/HCl, pH 7.4, 0.1 mg/ml NADH, and 2.5 mg/ml Nitrotetrazolium blue) or complex IV (0.5 mg/ml DAB, 50 mM phosphate buffer, pH 7.4, 20 µg/ml catalase, 1 mg/ml reduced cytochrome *c*, and 75 mg/ml sucrose) as described previously (Zerbetto et al., 1997).

### Quantification of mtDNA

Total DNA was isolated from hippocampus and striatum. Real-time amplification was performed using SYBR Green PCR Master Mix (Applied Biosystem). mtDNA was detected with primers specific for the murine *COI* gene. Amplification of the nuclear-encoded murine *RNaseP* gene was used as a reference. Relative abundance of mtDNA was determined using a comparative method ($2^{-\Delta\Delta Ct}$).

### In organello translation

Mitochondria were isolated from freshly dissected cerebral cortex. 500 µg mitochondria was resuspended in 500 µl translation buffer (100 mM mannitol, 10 mM sodium succinate, 80 mM KCl, 5 mM $MgCl_2$, 25 mM Hepes-KOH, pH 7.4, 1 mM KPi, pH 7.4, 5 mM ATP, 20 µM GTP, and 6 mM creatine phosphate) containing all amino acids (60 µg/ml) except methionine. Afterward, protein synthesis was performed for 1 h at 37°C in the presence of [$^{35}$S]Met (0.05 mCi/ml). Mitochondria were pelleted, resuspended in Laemmli buffer, and separated by SDS-PAGE. Newly synthesized mitochondrial proteins were visualized by autoradiography. The total radioactive signal was quantified using ImageJ.

### Statistical analysis

For statistical analyses, at least three independent experiments were performed. Data are represented as mean ± SD. Statistical significance was determined by *t* test.

### Online supplemental material

Fig. S1 shows the functional relationship of OMA1 with inflammatory and cell death pathways. Fig. S2 shows altered mitochondrial

morphology in *Phb2*$^{NKO}$*Oma1*$^{ko/ko}$ mice. Fig. S3 shows stabilization of mtDNA in the striatum of *Phb2*$^{NKO}$*Oma1*$^{ko/ko}$ mice and impaired mitochondrial translation in *Phb2*$^{NKO}$ and *Phb2*$^{NKO}$*Oma1*$^{ko/ko}$ mice. Online supplemental material is available at http://www.jcb.org/cgi/content/full/jcb.201507022/DC1.


### Acknowledgments

We thank Esther Barth and Helga Bank for excellent technical support, Shuaiyu Wang for help in immunohistochemistry, Dr. Gunter Rappl (Central Cell Sort Facility, Cologne, Germany) for help in flow cytometry, and Dr. Astrid Schauss (Cologne Excellence Cluster on Cellular Stress Responses in Aging-Associated Diseases imaging facility) for support in image acquisition.

This work was supported by an European Molecular Biology Organization long-term fellowship to R. Richter-Dennerlein and grants of the Deutsche Forschungsgemeinschaft and the European Research Council to T. Langer and by the Ministerio de Economía y Competitividad (Spain) to C. López-Otín. The Instituto Universitario de Oncología is supported by Fundación Bancaria Caja de Ahorros de Asturias. C. López-Otín is an Investigator of the Botín Foundation supported by Banco Santander through its Santander Universities Global Division.

The authors declare no competing financial interests.

Submitted: 6 July 2015
Accepted: 14 December 2015


## References


Akepati, V.R., E.C. Müller, A. Otto, H.M. Strauss, M. Portwich, and C. Alexander. 2008. Characterization of OPA1 isoforms isolated from mouse tissues. *J. Neurochem.* 106:372–383. http://dx.doi.org/10.1111/j.1471-4159.2008.05401.x

Almajan, E.R., R. Richter, L. Paeger, P. Martinelli, E. Barth, T. Decker, N.G. Larsson, P. Kloppenburg, T. Langer, and E.I. Rugarli. 2012. AFG3L2 supports mitochondrial protein synthesis and Purkinje cell survival. *J. Clin. Invest.* 122:4048–4058. http://dx.doi.org/10.1172/JCI64604

Anand, R., T. Wai, M.J. Baker, N. Kladt, A.C. Schauss, E. Rugarli, and T. Langer. 2014. The i-AAA protease YME1L and OMA1 cleave OPA1 to balance mitochondrial fusion and fission. *J. Cell Biol.* 204:919–929. http://dx.doi.org/10.1083/jcb.201308006

Baker, M.J., P.A. Lampe, D. Stojanovski, A. Korwitz, R. Anand, T. Tatsuta, and T. Langer. 2014. Stress-induced OMA1 activation and autocatalytic turnover regulate OPA1-dependent mitochondrial dynamics. *EMBO J.* 33:578–593. http://dx.doi.org/10.1002/embj.201386474

Burté, F., V. Carelli, P.F. Chinnery, and P. Yu-Wai-Man. 2015. Disturbed mitochondrial dynamics and neurodegenerative disorders. *Nat. Rev. Neurol.* 11:11–24. http://dx.doi.org/10.1038/nrneurol.2014.228

Cereghetti, G.M., A. Stangherlin, O. Martins de Brito, C.R. Chang, C. Blackstone, P. Bernardi, and L. Scorrano. 2008. Dephosphorylation by calcineurin regulates translocation of Drp1 to mitochondria. *Proc. Natl. Acad. Sci. USA.* 105:15803–15808. http://dx.doi.org/10.1073/pnas.0808249105

Cipolat, S., O. Martins de Brito, B. Dal Zilio, and L. Scorrano. 2004. OPA1 requires mitofusin 1 to promote mitochondrial fusion. *Proc. Natl. Acad. Sci. USA.* 101:15927–15932. http://dx.doi.org/10.1073/pnas.0407043101

Cipolat, S., T. Rudka, D. Hartmann, V. Costa, L. Serneels, K. Craessaerts, K. Metzger, C. Frezza, W. Annaert, L. D'Adamio, et al. 2006. Mitochondrial rhomboid PARL regulates cytochrome c release during apoptosis via OPA1-dependent cristae remodeling. *Cell.* 126:163–175. http://dx.doi.org/10.1016/j.cell.2006.06.021

Civiletto, G., T. Varanita, R. Cerutti, T. Gorletta, S. Barbaro, S. Marchet, C. Lamperti, C. Viscomi, L. Scorrano, and M. Zeviani. 2015. Opa1 overexpression ameliorates the phenotype of two mitochondrial disease mouse models. *Cell Metab.* 21:845–854. http://dx.doi.org/10.1016/j.cmet.2015.04.016

Cribbs, J.T., and S. Strack. 2007. Reversible phosphorylation of Drp1 by cyclic AMP-dependent protein kinase and calcineurin regulates mitochondrial fission and cell death. *EMBO Rep.* 8:939–944. http://dx.doi.org/10.1038/sj.embor.7401062

Desmurs, M., M. Foti, E. Raemy, F.M. Vaz, J.C. Martinou, A. Bairoch, and L. Lane. 2015. C11orf83, a mitochondrial cardiolipin-binding protein involved in bc1 complex assembly and supercomplex stabilization. *Mol. Cell. Biol.* 35:1139–1156. http://dx.doi.org/10.1128/MCB.01047-14

Ehses, S., I. Raschke, G. Mancuso, A. Bernacchia, S. Geimer, D. Tondera, J.C. Martinou, B. Westermann, E.I. Rugarli, and T. Langer. 2009. Regulation of OPA1 processing and mitochondrial fusion by m-AAA protease isoenzymes and OMA1. *J. Cell Biol.* 187:1023–1036. http://dx.doi.org/10.1083/jcb.200906084

Frezza, C., S. Cipolat, O. Martins de Brito, M. Micaroni, G.V. Beznoussenko, T. Rudka, D. Bartoli, R.S. Polishuck, N.N. Danial, B. De Strooper, and L. Scorrano. 2006. OPA1 controls apoptotic cristae remodeling independently from mitochondrial fusion. *Cell.* 126:177–189. http://dx.doi.org/10.1016/j.cell.2006.06.025

Friedman, J.R., and J. Nunnari. 2014. Mitochondrial form and function. *Nature.* 505:335–343. http://dx.doi.org/10.1038/nature12985

Griparic, L., T. Kanazawa, and A.M. van der Bliek. 2007. Regulation of the mitochondrial dynamin-like protein Opa1 by proteolytic cleavage. *J. Cell Biol.* 178:757–764. http://dx.doi.org/10.1083/jcb.200704112

He, J., H.M. Cooper, A. Reyes, M. Di Re, H. Sembongi, T.R. Litwin, J. Gao, K.C. Neuman, I.M. Fearnley, A. Spinazzola, et al. 2012. Mitochondrial nucleoid interacting proteins support mitochondrial protein synthesis. *Nucleic Acids Res.* 40:6109–6121. http://dx.doi.org/10.1093/nar/gks266

Head, B., L. Griparic, M. Amiri, S. Gandre-Babbe, and A.M. van der Bliek. 2009. Inducible proteolytic inactivation of OPA1 mediated by the OMA1 protease in mammalian cells. *J. Cell Biol.* 187:959–966. http://dx.doi.org/10.1083/jcb.200906083

Ishihara, N., Y. Fujita, T. Oka, and K. Mihara. 2006. Regulation of mitochondrial morphology through proteolytic cleavage of OPA1. *EMBO J.* 25:2966–2977. http://dx.doi.org/10.1038/sj.emboj.7601184

Jiang, X., H. Jiang, Z. Shen, and X. Wang. 2014. Activation of mitochondrial protease OMA1 by Bax and Bak promotes cytochrome c release during apoptosis. *Proc. Natl. Acad. Sci. USA.* 111:14782–14787. http://dx.doi.org/10.1073/pnas.1417253111

Kasashima, K., M. Sumitani, M. Satoh, and H. Endo. 2008. Human prohibitin 1 maintains the organization and stability of the mitochondrial nucleoids. *Exp. Cell Res.* 314:988–996. http://dx.doi.org/10.1016/j.yexcr.2008.01.005

Khandelwal, P.J., A.M. Herman, and C.E. Moussa. 2011. Inflammation in the early stages of neurodegenerative pathology. *J. Neuroimmunol.* 238:1–11. http://dx.doi.org/10.1016/j.jneuroim.2011.07.002

Meeusen, S., R. DeVay, J. Block, A. Cassidy-Stone, S. Wayson, J.M. McCaffery, and J. Nunnari. 2006. Mitochondrial inner-membrane fusion and crista maintenance requires the dynamin-related GTPase Mgm1. *Cell.* 127:383–395. http://dx.doi.org/10.1016/j.cell.2006.09.021

Merkwirth, C., S. Dargazanli, T. Tatsuta, S. Geimer, B. Löwer, F.T. Wunderlich, J.C. von Kleist-Retzow, A. Waisman, B. Westermann, and T. Langer. 2008. Prohibitins control cell proliferation and apoptosis by regulating OPA1-dependent cristae morphogenesis in mitochondria. *Genes Dev.* 22:476–488. http://dx.doi.org/10.1101/gad.460708

Merkwirth, C., P. Martinelli, A. Korwitz, M. Morbin, H.S. Brönneke, S.D. Jordan, E.I. Rugarli, and T. Langer. 2012. Loss of prohibitin membrane scaffolds impairs mitochondrial architecture and leads to tau hyperphosphorylation and neurodegeneration. *PLoS Genet.* 8:e1003021. http://dx.doi.org/10.1371/journal.pgen.1003021

Merrill, R.A., and S. Strack. 2014. Mitochondria: a kinase anchoring protein 1, a signaling platform for mitochondrial form and function. *Int. J. Biochem. Cell Biol.* 48:92–96. http://dx.doi.org/10.1016/j.biocel.2013.12.012

Mishra, P., and D.C. Chan. 2014. Mitochondrial dynamics and inheritance during cell division, development and disease. *Nat. Rev. Mol. Cell Biol.* 15:634–646. http://dx.doi.org/10.1038/nrm3877

Mishra, P., V. Carelli, G. Manfredi, and D.C. Chan. 2014. Proteolytic cleavage of Opa1 stimulates mitochondrial inner membrane fusion and couples fusion to oxidative phosphorylation. *Cell Metab.* 19:630–641. http://dx.doi.org/10.1016/j.cmet.2014.03.011

Oettinghaus, B., J.M. Schulz, L.M. Restelli, M. Licci, C. Savoia, A. Schmidt, K. Schmitt, A. Grimm, L. More, J. Hench, et al. 2016. Synaptic dysfunction, memory deficits and hippocampal atrophy due to ablation of mitochondrial fission in adult forebrain neurons. *Cell Death Differ.* 23:18–28.

Olichon, A., L. Baricault, N. Gas, E. Guillou, A. Valette, P. Belenguer, and G. Lenaers. 2003. Loss of OPA1 perturbates the mitochondrial inner membrane structure and integrity, leading to cytochrome c release and apoptosis. *J. Biol. Chem.* 278:7743–7746. http://dx.doi.org/10.1074/jbc.C200677200

Ong, S.B., A.R. Hall, and D.J. Hausenloy. 2013. Mitochondrial dynamics in cardiovascular health and disease. *Antioxid. Redox Signal.* 19:400–414. http://dx.doi.org/10.1089/ars.2012.4777

Osman, C., C. Merkwirth, and T. Langer. 2009. Prohibitins and the functional compartmentalization of mitochondrial membranes. *J. Cell Sci.* 122:3823–3830. http://dx.doi.org/10.1242/jcs.037655

Osman, C., D.R. Voelker, and T. Langer. 2011. Making heads or tails of phospholipids in mitochondria. *J. Cell Biol.* 192:7–16. http://dx.doi.org/10.1083/jcb.201006159

Patten, D.A., J. Wong, M. Khacho, V. Soubannier, R.J. Mailloux, K. Pilon-Larose, J.G. MacLaurin, D.S. Park, H.M. McBride, L. Trinkle-Mulcahy, et al. 2014. OPA1-dependent cristae modulation is essential for cellular adaptation to metabolic demand. *EMBO J.* 33:2676–2691. http://dx.doi.org/10.15252/embj.201488349

Pfeiffer, K., V. Gohil, R.A. Stuart, C. Hunte, U. Brandt, M.L. Greenberg, and H. Schägger. 2003. Cardiolipin stabilizes respiratory chain supercomplexes. *J. Biol. Chem.* 278:52873–52880. http://dx.doi.org/10.1074/jbc.M308366200

Polykratis, A., N. Hermance, M. Zelic, J. Roderick, C. Kim, T.M. Van, T.H. Lee, F.K. Chan, M. Pasparakis, and M.A. Kelliher. 2014. Cutting edge: RIPK1 Kinase inactive mice are viable and protected from TNF-induced necroptosis in vivo. *J. Immunol.* 193:1539–1543. http://dx.doi.org/10.4049/jimmunol.1400590

Quirós, P.M., A.J. Ramsay, D. Sala, E. Fernández-Vizarra, F. Rodríguez, J.R. Peinado, M.S. Fernández-García, J.A. Vega, J.A. Enríquez, A. Zorzano, and C. López-Otín. 2012. Loss of mitochondrial protease OMA1 alters processing of the GTPase OPA1 and causes obesity and defective thermogenesis in mice. *EMBO J.* 31:2117–2133. http://dx.doi.org/10.1038/emboj.2012.70

Quirós, P.M., T. Langer, and C. López-Otín. 2015. New roles for mitochondrial proteases in health, ageing and disease. *Nat. Rev. Mol. Cell Biol.* 16:345–359. http://dx.doi.org/10.1038/nrm3984

Richter-Dennerlein, R., A. Korwitz, M. Haag, T. Tatsuta, S. Dargazanli, M. Baker, T. Decker, T. Lamkemeyer, E.I. Rugarli, and T. Langer. 2014. DNAJC19, a mitochondrial cochaperone associated with cardiomyopathy, forms a complex with prohibitins to regulate cardiolipin remodeling. *Cell Metab.* 20:158–171. http://dx.doi.org/10.1016/j.cmet.2014.04.016

Roy, M., P.H. Reddy, M. Iijima, and H. Sesaki. 2015. Mitochondrial division and fusion in metabolism. *Curr. Opin. Cell Biol.* 33:111–118. http://dx.doi.org/10.1016/j.ceb.2015.02.001

Schlame, M. 2013. Cardiolipin remodeling and the function of tafazzin. *Biochim. Biophys. Acta.* 1831:582–588. http://dx.doi.org/10.1016/j.bbalip.2012.11.007

Shields, L.Y., H. Kim, L. Zhu, D. Haddad, A. Berthet, D. Pathak, M. Lam, R. Ponnusamy, L.G. Diaz-Ramirez, T.M. Gill, H. Sesaki, L. Mucke, and K. Nakamura. 2015. Dynamin-related protein 1 is required for normal mitochondrial bioenergetic and synaptic function in CA1 hippocampal neurons. Cell Death Dis. 6:e1725.

Song, Z., H. Chen, M. Fiket, C. Alexander, and D.C. Chan. 2007. OPA1 processing controls mitochondrial fusion and is regulated by mRNA splicing, membrane potential, and Yme1L. *J. Cell Biol.* 178:749–755. http://dx.doi.org/10.1083/jcb.200704110

Stiburek, L., J. Cesnekova, O. Kostkova, D. Fornuskova, K. Vinsova, L. Wenchich, J. Houstek, and J. Zeman. 2012. YME1L controls the accumulation of respiratory chain subunits and is required for apoptotic resistance, cristae morphogenesis, and cell proliferation. *Mol. Biol. Cell.* 23:1010–1023. http://dx.doi.org/10.1091/mbc.E11-08-0674

Tatsuta, T., K. Model, and T. Langer. 2005. Formation of membrane-bound ring complexes by prohibitins in mitochondria. *Mol. Biol. Cell.* 16:248–259. http://dx.doi.org/10.1091/mbc.E04-09-0807

Tondera, D., S. Grandemange, A. Jourdain, M. Karbowski, Y. Mattenberger, S. Herzig, S. Da Cruz, P. Clerc, I. Raschke, C. Merkwirth, et al. 2009. SLP-2 is required for stress-induced mitochondrial hyperfusion. *EMBO J.* 28:1589–1600. http://dx.doi.org/10.1038/emboj.2009.89

Varanita, T., M.E. Soriano, V. Romanello, T. Zaglia, R. Quintana-Cabrera, M. Semenzato, R. Menabò, V. Costa, G. Civiletto, P. Pesce, et al. 2015. The OPA1-dependent mitochondrial cristae remodeling pathway controls atrophic, apoptotic, and ischemic tissue damage. *Cell Metab.* 21:834–844. http://dx.doi.org/10.1016/j.cmet.2015.05.007

Xiao, X., Y. Hu, P.M. Quirós, Q. Wei, C. López-Otín, and Z. Dong. 2014. OMA1 mediates OPA1 proteolysis and mitochondrial fragmentation in experimental models of ischemic kidney injury. *Am. J. Physiol. Renal Physiol.* 306:F1318–F1326. http://dx.doi.org/10.1152/ajprenal.00036.2014

Youle, R.J., and A.M. van der Bliek. 2012. Mitochondrial fission, fusion, and stress. *Science.* 337:1062–1065. http://dx.doi.org/10.1126/science.1219855

Zerbetto, E., L. Vergani, and F. Dabbeni-Sala. 1997. Quantification of muscle mitochondrial oxidative phosphorylation enzymes via histochemical staining of blue native polyacrylamide gels. *Electrophoresis.* 18:2059–2064. http://dx.doi.org/10.1002/elps.1150181131

Zhang, K., H. Li, and Z. Song. 2014. Membrane depolarization activates the mitochondrial protease OMA1 by stimulating self-cleavage. *EMBO Rep.* 15:576–585. http://dx.doi.org/10.1002/embr.201338240